17th World Conference on Earthquake Engineering, 17WCEE
Sendai, Japan - September 13th to 18th 2020

PROBING SEISMIC REINFORCEMENT EFFECT OF A WOODEN HOUSE BASED ON AMBIENT VIBRATION MEASUREMENTS

K. Iiyama [(1)], M. Aikawa [(2)], H. Morikawa [(3)] and O. Kockaya [(4)]

[(1)] *Assistant Professor, Tokyo Institute of Technology, iiyama.k.aa@m.titech.ac.jp*
[(2)] *Former undergraduate student, Tokyo Institute of Technology*
[(3)] *Professor, Tokyo Institute of Technology, morikawa.h.aa@m.titech.ac.jp*
[(4)] *Teaching assistant, Middle East Technical University, kockaya@metu.edu.tr*

Abstract

Considering a lot of wooden structures in Japan and in particular, around 90 % of detached residences are wooden houses, structural-performance estimation of wooden houses is essential. A wooden house generally consists of many timbers, such as pillars, beams, floors, and walls, and they are connected with, that is a so-called wooden framework. Iron nails, bolts, and seismic brackets can also be attached to some joints to improve the seismic performance of the structure. The performance of such a complex structure can basically be diagnosed according to the guidelines for seismic diagnosis and repairment, which provides not only the structure strength of each member for each material type, timber size, joint condition and so on, but also the relationships between force and deformation for representative bearing components, based on push-over test and ditto numerical analysis. It is, however, generally a task to get the whole information on material and structural properties after its completion, and that makes it difficult to assess the structural state of existing wooden houses.

Ambient vibration measurement is one of the possible ways to estimate the current state of existing structures. Although the residual strength estimation from the measurement records is challenging, the modal propreties such as natural frequency, mode shape and damping factor can be easily identified from the records at several sites on a targeted structure. Since the change in fundamental frequency has particulary high sensitivity to the rigidity of a structure, the ambient vibration measurement are often conducted before and after events, to evaluate the state of the structure. The effect of each structural member on the change in frequency are, however, veiled as long as focusing only on frequency information, and hence the practicality of ambient vibration records for structural state assessment remains uncertain. To examine the relationship between the seismic reinforcement effect of a wooden house and modal properties more properly, modal identification based on three-dimensional vibrational characteristics is significance, and then both the measurement-based and the model-based approaches is indispensable.

In this study, we conducted ambient vibration measurements for a two-story wooden house during the process of applying seismic reinforcement, that is, 1) before installation of seismic brackets, 2) after installation of seismic brackets, 3) after installation of walls, and 4) after the completed state. 12 to 14 velocity sensors were used in each process. Using the horizontal components of the records, the natural frequency, mode shape and perticipation factor were identified through the frequency domain decomposition (FDD) technique, and the change in modal parameters due to the difference in seismic reinforcement process was revealed. To demonstrate the validity of the results based on the measurements, three-dimensional numerical models consist of pillars, beams, floors, and walls and their joints are examined, by comparing the modal properties with that identified from the measurement records. Although some aspects of the observation-based modal properties could not be reproduced, the differences in the structural characteristics of each of the reinforcement work stages 1) to 4) were successfully explained.

Keywords: Wooden house, Ambient vibration, FDD technique, Seismic reinforcement effect, Parameter identification

1. Introduction

As there is a lot of wooden-type residential houses in Japan, structural-performance estimation of wooden houses is essential. The seismic performance of wooden houses can be evaluated according to the guidelines for seismic diagnosis and repair by the experts. However, it is generally a task to get full information on material and structural properties after its completion, and that makes it difficult to assess the structural state of existing wooden houses. Ambient vibration/Microtremor does not directly give information on the strength of existing structures, whereas it gives information on the dynamic properties to some extent. Many studies, which focused on ambient vibration measurements, had been done for a long time, e.g., [1]-[4], and it seems that their objects have been shifted from modeling of wooden structures or examining their rigidity to evaluating the seismic performance, e.g., [5]-[8]. Some of them indicated that the predominant frequency has a relationship with building year, and modal parameters identified from microtremor records can be utilized for seismic diagnosis. Simple mode shapes have been also utilized to estimate the rigidity of the structure.

The advantage of eigenfrequencies is in its simplicity and robustness. Although it only gives limited information on the structural state, it is often employed as a representative index. Whereas, there are few studies focused on detailed modal properties of existing wooden houses. Using multiple sensors, it might be possible to identify the three-dimensional vibrational characteristics, and examine the relationship between the vibrational characteristics and the structural state of the target structure. In addition, to confirm the reliability of the identification results, both the measurement-based and the model-based approaches are desirable.

This paper shows the detailed modal properties of a two-story wooden house based on multi-point simultaneous measurements, targets for different construction stages. The difference in modal properties identified for each reinforcement process is demonstrated. The reliability of the identification results is also examined. Moreover, we make three-dimensional numerical models for each reinforcement process based on limited information of actual structural state, and perform eigenvalue analysis. Through the comparison between the measurement-based modal properties and the numerical-based ones, the utilization of the ambient vibration measurements is discussed.

2. Object structure and observation

2.1 Outline of object structure and seismic reinforcement work

The object structure is a two-story wooden house, constructed in 1995 by the conventional-framework method. Fig. 1 shows the completion drawing of the object house with a small embankment under the foundation. For the purpose of renovation and seismic reinforcement, construction works had been carried out from July to October in 2016. As shown in Fig. 2, most of the walls and floors were removed until August 5th, except for the two rooms: the southwest corner room in the first floor (1F, the soundproof room) and the east room in the second floor (2F). Subsequently, some earthquake resistant metal fittings were attached until August 7th, the perimeter walls were constructed until August 11th. The outer walls, floors, and inner walls were lastly installed until October 25th.

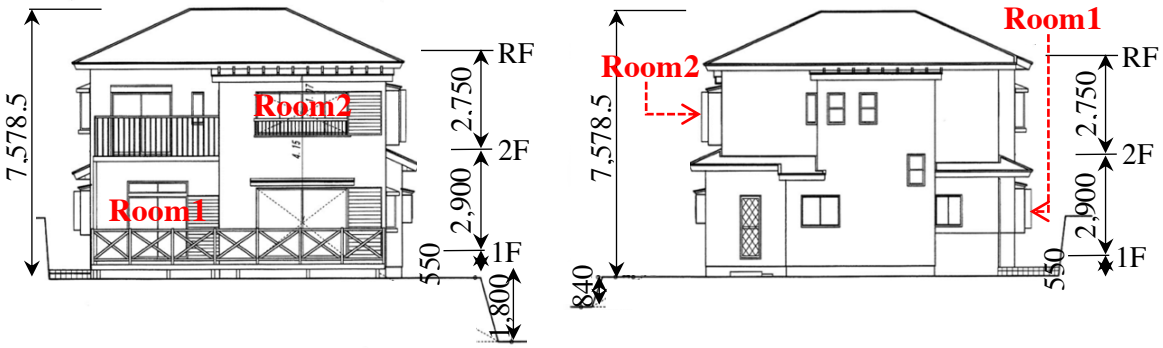

Fig. 1 – Completion figures for the south-side elevation (left) and for the north-side elevation (right)

Fig. 2 – photo images during the construction work: columns at 1F on Aug. 5th(left), a joint at 1F on Aug. 7th (left middle), outer wall on Aug. 11st[11] (right middle), and a room at 1F on Oct. 25th (right)

As mentioned above, the two rooms represented as "Room1" and "Room2" in Fig.1 were left as they were: their walls did not have removed during the construction work, although only the flooring of the east room in 2F was removed before Obs. 1.

2.2 Observation of ambient vibration for different construction stages

During the construction work, we observed ambient vibrations using the moving-coil type three component velocimeters (KVS-300, by Kinkei system Co.) and data loggers (OTK and AK, by alab Inc.). The sampling rates of OTK and AK are 200 Hz and 100 Hz, respectively. All the records were synchronized using GPS clock system just before each observation.

Four times multi-point simultaneous measurements are conducted: 1) before installation of seismic brackets, 2) after installation of seismic brackets, 3) after installation of walls, and 4) after the completed state. The outline of the observations is shown in Table 1. The sensor arrangement for each observation is shown in Fig. 3, where the suffix numbers *X* (e.g. OTK*X*, AK*X*) in the figure denotes the unique number for each logger. As shown in Fig. 3, we used 12 sensors by the same arrangement for the three observations in August (red circles), and rearranged them on October 25th (blue squares) with extra two sensors. Hereafter, these four observations are referred to as "Obs.1", "Obs.2", "Obs.3", and "Obs.4" respectively for the observation on August 5th, August 7th, August 11th, and October 25th.

As mentioned above, the two rooms represented as "Room1" and "Room2" in Fig. 3 were almost left as it was: their walls did not have removed during the construction work, although only the flooring of Room2 was removed before Obs. 1.

Table 1 – Outline of observation and analysis

	Date and recording time	**Construction details**	**Weather**	**Number of components for analysis**	**Block length and number for analysis**
Obs. 1	Aug. 5th, 2016 2:30 - 3:30 (60 min.)	Initial state (Most of walls and floors were removed)	Sunny, light breeze	24 (12 sensors)	40 sec * 31 blocks
Obs. 2	Aug. 7th, 2016 17:15 - 18:15 (60 min.)	Attaching of a part of earthquake resistant metal fittings	Ditto	Ditto	40 sec * 13 blocks
Obs. 3	Aug. 11th, 2016 19:35 - 20:45 (70 min.)	Attaching the perimeter walls	Ditto	Ditto	40 sec * 24 blocks
Obs. 4	Oct. 25th, 2016 21:45 - 23:00 (75 min.)	Completion (Attaching floors and inner, outer walls)	Light rain, light breeze	28 (14 sensors)	40 sec * 19 blocks

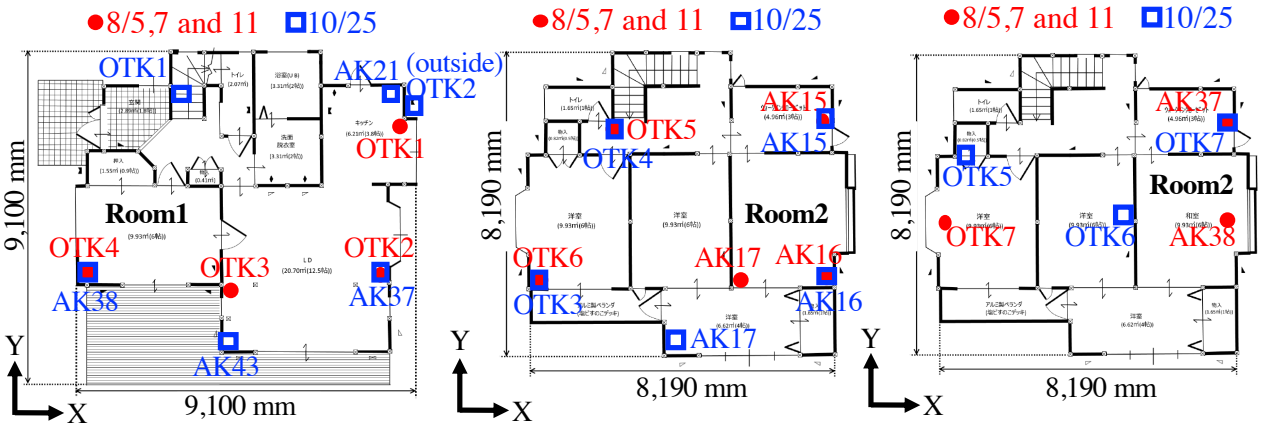

Fig. 3 – Sensor arrangement for each observation: on the floor of 1F (left), on the floor of 2F (middle) andon the ceiling beam or ceiling floor corresponding to the roof level (right)

3. Modal identification and consideration of its property

3.1 Method

Applying the frequency domain decomposition (FDD) technique [9], the modal frequencies and the corresponding mode shapes of the object structure were identified to examine the change in modal property for different structural state. The process of the FDD technique is simple; making the power spectrum density (PSD) matrix for each discretized frequency, and decomposing it through the singular value decomposition (SVD). The power-cross spectrum matrix is defined as the following.

$$[G_{yy}(\omega)] =< \boldsymbol{Y}^*(\omega)\boldsymbol{Y}(\omega)^T >, \quad \boldsymbol{Y}(\omega) = \{Y_1(\omega), \dots, Y_N(\omega)\}^T \tag{1}$$

where $Y_i(\omega)$ is the system response for i-th component in frequency domain, the superscript * and T respectively denote complex conjugate and transpose, and the symbol < > represents ensemble average. This study used only horizontal components of the records, N accordingly takes 24 and 28 respectively for the first three observations and the last observations. Based on vibration theory, the matrix can be approximated by the following, around the predominant modal frequencies which is represented as $sub(\omega)$,

$$[G_{yy}(\omega)] \approx \sum_{k \in sub(\omega)} \frac{d_k}{j\omega - \lambda_k} \boldsymbol{\varphi}_k^* \boldsymbol{\varphi}_k{}^T \tag{2}$$

where $\boldsymbol{\varphi}_k, \lambda_k$ are the mode shape vector and the pole for k-th mode, and d_k is the coefficient relates to k-th modal mass, modal damping and the pole. Since $[G_{yy}]$ is Hermitian matrix, it can be decomposed by SVD:

$$[G_{yy}] = \sum_i s_i \boldsymbol{u}_i \boldsymbol{u}_i^H, \quad s_1 > s_2 > \cdots > s_N \tag{3}$$

where superscript H is complex conjugate and transpose, s_i and $\boldsymbol{u}_i$ are the i-th singular value and the i-th singular vector, respectively. Based on the singular value spectrum, which is drawn by means the is drawn with the singular values for discretized frequencies, can be obtained by drawing the s_1 over the target frequency range, the possible eigenfrequencies are identified by peak picking, and the possible mode shapes are identified as the corresponding singular vector.

3.2 Identification of modal frequency and mode shape

Figure 4 shows the first singular spectrum $s_1(\omega)$ for all observations. Some peaks are found in each $s_1(\omega)$, in particular, three peaks for Obs.3 around 5 Hz, 6.5 Hz, and 8.7 Hz are distinct. On the other hand, some peaks are jagged: e.g., in the range from 7 Hz to 8 Hz for Obs.1 (red line), from 3 Hz to 4.5 Hz for Obs.2 (orange line), and from 8 Hz to 9 Hz for Obs.4 (blue line). To distinguish between some peaks derived from a different mode is generally problematic.

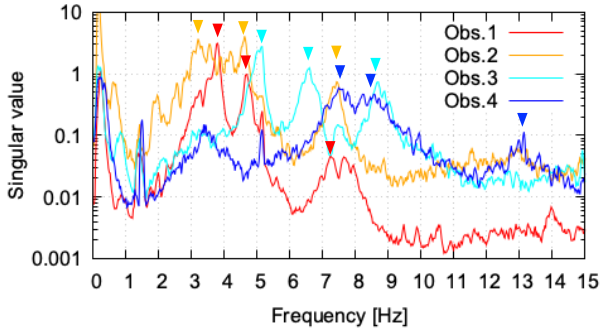

Fig. 4 – The first singular spectrum and the selected peaks

One of the ways to distinguish mode types is examining the transition of singular vectors. We focus on the transition of the first singular vector, hereafter we call it the first singular spectrum: $\boldsymbol{u}_1(\omega)$. Fig. 5 shows each element of $\boldsymbol{u}_1(\omega)$ (Fig. 5, upper panels) and the phase angle (Fig. 5, lower panels) for Obs.1. The upper panels of Fig. 5 are represented by $|u_{1i}|$ with the sign of $Re(u_{1i})$, where *Re* denotes real part and *i* represents the component number. From the figure, the changes in mode are clearly found ,for example, around at 4.2 Hz and 6.0 Hz. As for the range from 7 to 8 Hz, in which $s_1(\omega)$ jags, although small jumps can be found around 7.5 Hz in the upper-right panel of Fig. 5, the transitions of mode and phase are relatively stable. Moreover, although the phase of AK17 in the Y-direction clearly changes (yellow dots of lower right panel of Fig. 5), its $|u_{1i}|$ is close to zero (yellow line in upper right panel of Fig. 5). These characteristics indicate that the dynamic properties in the vicinity of 7.5 Hz are thought to be similar. Thus, it is possible to roughly divide the frequency range into mode categories, using the singular spectrum.

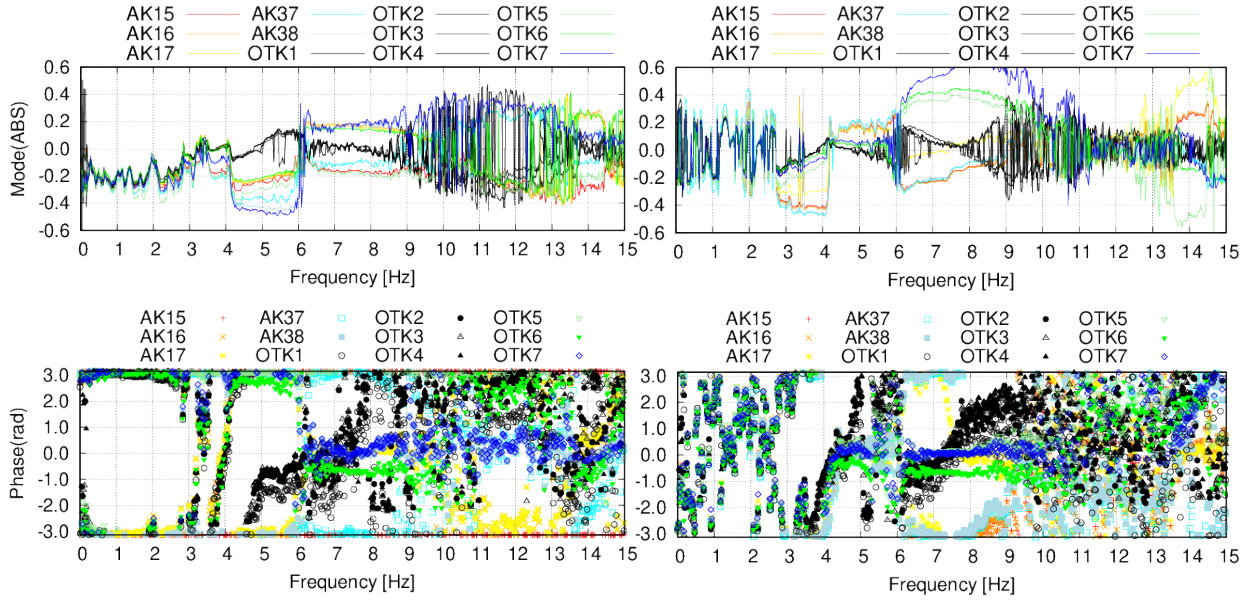

Fig. 5 – Transition of amplitude and phase of the first singular vector (ex. Aug. 5th) : $|u_{1i}|$ for X-direction (upper, left), $|u_{1i}|$ for Y-direction (upper, right), phase angle of $|u_{1i}|$ for X-direction (lower, left) and phase angle of $|u_{1i}|$ for Y-direction (lower, right)

We selected three representative frequencies for each observation case as follows: Firstly, selecting the dominant peaks of $s_1(\omega)$ as the potential frequency range. If the peak is clear and mode-like, select the corresponding frequency as a mode. If not, we divide the frequency range into mode categories based on the first singular vector spectrum $\boldsymbol{u}_1(\omega)$. After that, a maximum peak of $s_1(\omega)$ is selected as a mode from a divided frequency range. The selected peaks are shown in Fig. 4 by the inverted triangles. Hereafter, the corresponding frequency of *n*-th peak for Obs.*m* is referred as $f_n^{\mathrm{Obs}m}$.

Fig. 6 shows the corresponding $\boldsymbol{u}_1$ to the selected peaks for each observation. The corresponding frequencies are $(f_1^{\text{Obs1}}, f_2^{\text{Obs1}}, f_3^{\text{Obs1}}) = (3.78\text{ Hz}, 4.69\text{ Hz}, 7.23\text{ Hz})$, $(f_1^{\text{Obs2}}, f_2^{\text{Obs2}}, f_3^{\text{Obs2}}) = (3.20\text{ Hz}, 4.61\text{ Hz}, 7.42\text{ Hz})$, $(f_1^{\text{Obs3}}, f_2^{\text{Obs3}}, f_3^{\text{Obs3}}) = (5.13\text{ Hz}, 6.59\text{ Hz}, 8.69\text{ Hz})$ and $(f_1^{\text{Obs4}}, f_2^{\text{Obs4}}, f_3^{\text{Obs4}}) = (7.50\text{ Hz}, 8.57\text{ Hz}, 13.1\text{ Hz})$. From the appearance, we roughly divided these vectors into four mode types, that is, the eccentric-rotational mode, translational mode for the X- and Y directions, and rotational mode. The mode types and the corresponding frequencies are summarized in Table 2 with the ratio of frequencies. Hereafter, we represent these four mode types as V_{eR}, V_{Tx}, V_{Ty}, and V_{R}, respectively.

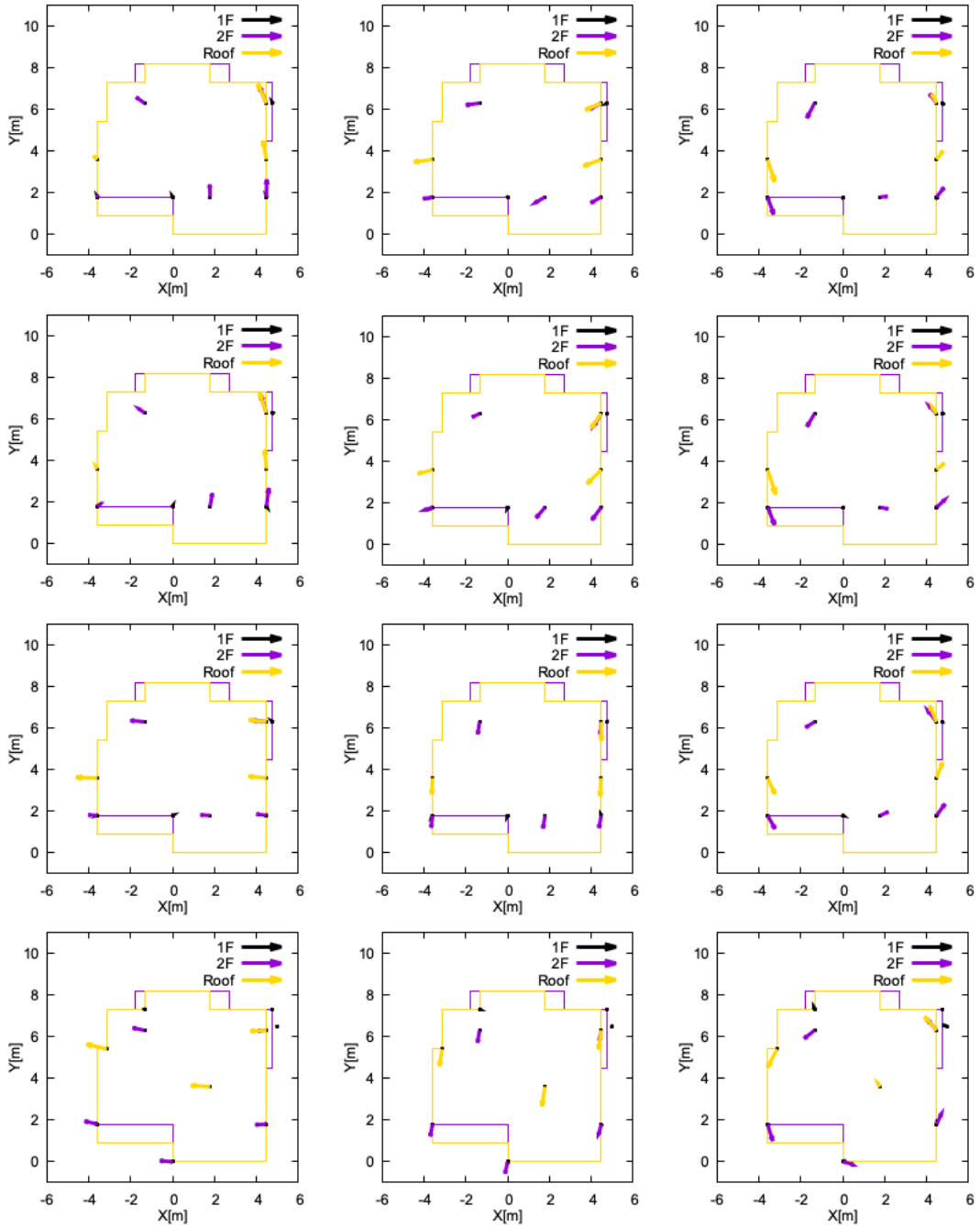

Fig. 6 – The first singular vectors corresponding to three representative frequencies: At the first frequency (left), the second one (middle) and the third one (right), for Obs.1 (upper panels), for Obs.2 (second upper panels), for Obs.3 (third upper panels) and for Obs.4 (bottom panels).

Table 2 – Selected frequency (Unit: Hz) and the increasing rate of frequency

Mode type	Obs.1	Obs.2	Obs.3	Obs.4	< Obs.3/Obs.2 >	< Obs.4/Obs.3 >
Eccentric rotation : V_{eR}	3.78	3.20	-	-		
Translation X : V_{Tx}	4.69	4.61	5.13	7.50	<1.11>	<1.46>
Translation Y : V_{Ty}	-	-	6.59	8.57		<1.30>
Rotation : V_R	7.23	7.42	8.69	13.1	<1.17>	<1.51>
< V_R / V_{Tx} >	<1.54>	<1.61>	<1.69>	<1.74>		

* < > represents the increasing rate of frequencies.

3.3 Change in mode frequency

The change in frequency before and after a certain event is often used as an indicator for structure evaluation, because the global rigidity of the structure gets directly reflected in it. The change in modal frequency for each mode type is shown in Fig. 7. The frequency obviously becomes higher after Obs.2, regardless of mode type. Comparing before and after the installation of perimeter walls: Obs.2 and Obs.3, the increasing rate of frequency for V_{Tx} and V_R are 11% and 17%, respectively. Further, comparing before and after the completion construction: Obs.3 and Obs.4, the increasing rate of frequency for V_{Tx}, V_{Ty} and V_R are of 46%, 30% and 51%, respectively. Moreover, the increase of ratios of V_R to V_{Tx} are 7%, 8%, and 5% and this means the rotation constraint also became stronger due to settings of walls and floors.

Although the absolute global rigidity cannot be estimated, the mass increased during the construction work and the change in global rigidity seems larger than those calculated from the above rate.

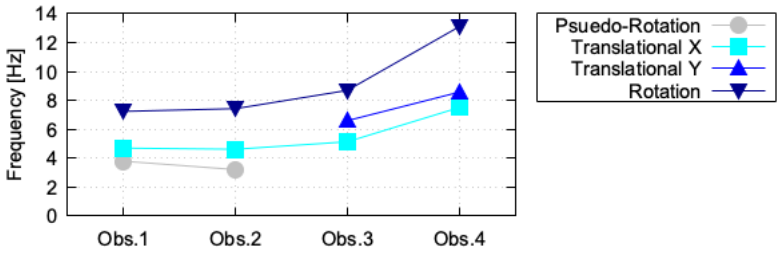

Fig. 7 – Change in frequency for each mode type

3.3 Modal characteristics

From Fig. 6, the three mode shapes between Obs.1 and Obs.2 and between Obs.3 and Obs.4 are respectively resemble each other. Actually, the values of the modal assurance criterion (MAC)[10] between three modes for Obs.1 and Obs.2 are respectively 0.968, 0.814, and 0.967. This indicates the vectors between Obs.1 and Obs.2, both are before outer wall installation, are very close. Moreover, although around the first peak of the singular value for Obs. 2 are jagged, the corresponding mode shapes from 3 Hz to 3.8 Hz are close each other. These suggest that the dynamic characteristics between Obs.1 and Obs.2 are almost the same, that is, the effect of the installation of some earthquake resistant metal fittings on modal properties is limited.

The following characteristics are also found in the figure: 1) the mode at f_1^{Obs1} and f_1^{Obs2} are similar eccentric rotation, 2) the mode type at f_1^{Obs3} and f_1^{Obs4} show translational mode for the X-direction, at f_2^{Obs3} and f_2^{Obs4} show translational mode for the Y-directions, 3) the rotational mode for all observations. It is inferred the eccentricity of the rotational mode at f_1^{Obs1} and f_1^{Obs2} is strongly related to the rigid section in 1F: Room1, the walls and the floor of which were remaining. Based on the mode shapes, the dynamic properties seem to be more stable after perimeter wall installation, and the strengthen are improved by completing all floors, inner walls and outer walls.

On the other hand, in terms of the translational modes for Obs.3 and Obs.4, the amplitude and the angle of different positions on the same floor are slightly different. It indicates that rigid floor assumption does not hold even if after completion, and the error should be count when estimates mode shapes from a few sensors.

4. Attempt to construct reasonable numerical model

In Chapter 3, we identified the modal properties for the different construction stages and showed the change in the eigenfrequency and the corresponding mode shape for three representative modes. The cause of the differences in eigenfrequency and mode shape can be qualitatively estimated based on the progression status of the construction. In this chapter, we attempt to construct detailed numerical model which can estimates the modal properties of actual structure. Firstly, numerical models are constructed. Adjusting the model parameters, the modal properties are calculated through eigenvalue analysis using the numerical models. Subsequently, the modal properties are compared to those shown in Fig. 6. We also discuss how to utilize modal properties identified.

4.1 Construction of numerical model

Although it is desirable to construct a close-to-reality model, it is generally a task due to the lack of information on parameters of a target structure. Here, we make frame-models using limited information. The positions of columns and beams are determined based on the completion drawings (Fig. 4). The presence of floors, inner- and outer-walls are determined by referring both the completion drawings and the photos of each construction stage. The main column and beam of the size of 12.0 *12.0 cm^2, the diagonal bracing of 10.5 *5 cm^2. The walls, floors and roofs, the size and the structure of which are unclear, are roughly modeled as beam members. The cross-section sizes of the beam members are determined according to their setting positions.

The parameters of material were almost unknown. We accordingly employed many assumptions: The standard Young's modulus E_{ws} and the unit weight u_{ws} are 700 kN/cm^2 and 10 kN/m^3. The horizontal members attached to the ground is made of concrete, and the Young's modulus E_c and the unit weight u_c are 2,100 kN/cm^2 and 21 kN/m^3. For the windows, the doors, and the roof members, extra weights are added. The outermost beams of the Young's modulus are set as larger value of E_{ws}, instead of rigid bar. The ground springs are also installed at the basement nodes.

Since the modal properties for Obs.1 and Obs.2 are very similar, we employ three models for Obs.1, Obs.3 and Obs.4. Adding the perimeter walls to the model for Obs. 1, the model for Obs. 3 is made. Adding the remaining floors and outer walls to the model for Obs.3, the model for Obs.4 is created. The shapes of model are shown in Fig. 8. As shown in the figure, the walls are roughly modeled by bracing member in this study.

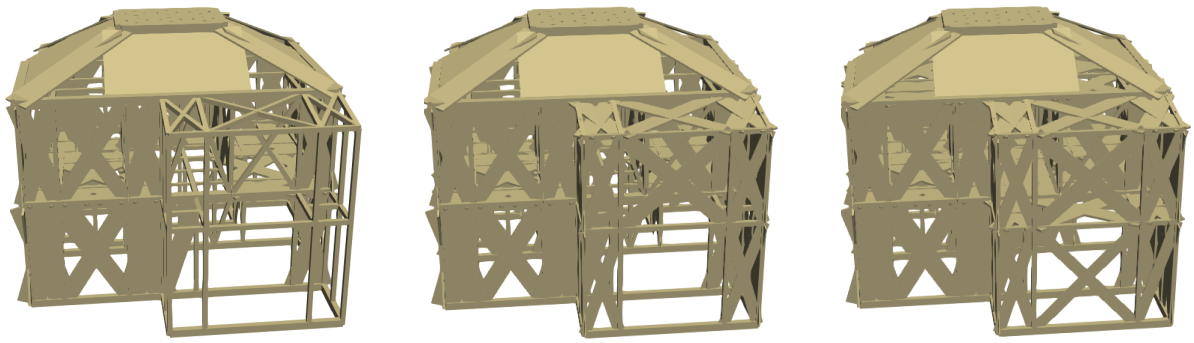

Fig. 8 – Appearance of numerical models corresponding to Obs.1 (left), Obs.2 (middle) and Obs.4 (right)

4.2 Results and comparison of modal properties

Overall, the calculated eigenfrequencies using the above models are higher than the observation-based identified frequencies. To adjust the eigenfrequency, we simply added extra constant masses to all nodes. The extra masses added for the models for Obs.1 and Obs.3 is two times larger than that for Obs.4. This might be due to the existence of scaffoldings constructed around the house.

Table 3 shows the first to third eigenfrequencies calculated from eigenvalue analysis after adding the extra masses. The observation-based frequencies and the ratio of these frequencies shown in Table 2 are also

shown in the figure. According to Table 3, the differences of frequencies are less than 7% and it seems to be agreeable.

Table 3 – Eigenfrequencies based on observation-based and numerical analysis-based calculations (Unit: Hz)

Method	**FDD analysis using observation records**			**Eigenvalue analysis using numerical model**		
Mode type \ Observation	**Obs.1**	**Obs.3**	**Obs.4**	**Obs.1**	**Obs.3**	**Obs.4**
Eccentric rotation : V_{eR}	3.78	-	-	3.84 (1.02)	-	-
Translation X : V_{Tx}	4.69	5.13	7.50	4.98 (1.06)	5.31 (1.04)	7.60 (1.01)
Translation Y : V_{Ty}	-	6.59	8.57	-	6.29 (0.95)	8.63 (1.01)
Rotation : V_{R}	7.23	8.69	13.1	7.15 (0.99)	8.67 (1.00)	12.2 (0.93)

The first- to third-order mode shapes are shown in Fig. 9. The vector-elements are represented by using only the nodes corresponding to the sensor position. Overall, the mode types in the figure coincide with those shown in Fig. 6. The MAC values between the numerical-based and the observation-based mode shapes, for the first-, second-, and third-order mode, are respectively (0.98, 0.92, 0.82) for Obs.1, (0.97, 0.97, 0.96) for Obs.3, and (0.91, 0.93, 0.84) for Obs.4. They are averagely high enough, although several values are less than 0.9. It indicates that these numerical models seem to be agreeable to explain the dynamic properties of the actual structures, whereas these models are just one of the local solutions.

According to the model, the eccentric mode found at both f1Obs1 and f1Obs2 seems to be derived from the existence of Room1. After installing the perimeter, the unbalance is improved. On the other hand, the change in mode shapes is not apparent after the installation of all floors and finishing walls. It implies the difficulty of identifying damage at the floor or finishing-wall from the change in mode shapes, even if the damage is severe, and even if more than ten sensors are employed.

4.3 About utilization of measurement records and modal identification

The parameters which determines modal property consists of mass and rigidity, and their combination. In this study, we added extra mass to adjust the eigenfrequencies. However, the total masses of the models before adding extra mass were respectively around 49, 69 and 73 tons for Obs.1, Obs.3 and Obs.4 and they seemed too large according to the current research [11], even if the concrete foundation of about 5 ton are considered. When we utilize modal properties to discuss the rigidity of elements, mass estimation with good accuracy is indispensable. Some methodology to estimate the mass distribution was proposed, for instance, the method using participation factors [12]. The participation factors can be identified using some time-domain techniques [e.g.,13]. Thus, there is room for improvement of numerical models.

On the other hand, the number of sensors for measurement are generally limited. As is obvious, the numerical model determined in this study is nothing more than one of the local solutions. In addition, the measurement records necessarily include various noises. Moreover, as shown in Fig. 5, the mode at peaks of the singular value spectrum is not just same as the mode at adjacent frequency. These suggest that we should consider the identified frequencies, mode shapes, and no matter of course damping factors, include errors to some extent, and then we can utilize the rough frequency change and the mode-types.

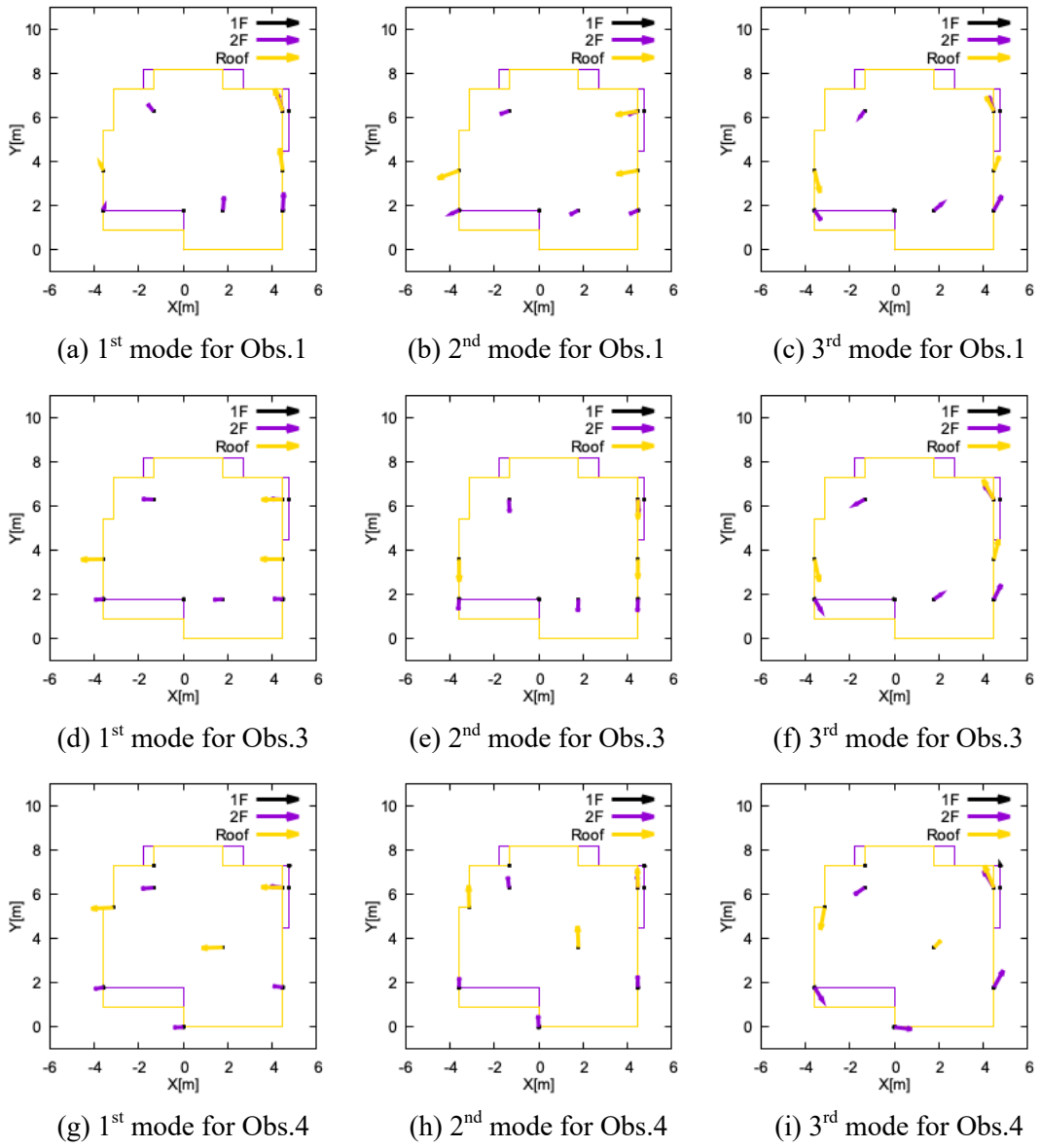

(a) 1st mode for Obs.1 (b) 2nd mode for Obs.1 (c) 3rd mode for Obs.1

(d) 1st mode for Obs.3 (e) 2nd mode for Obs.3 (f) 3rd mode for Obs.3

(g) 1st mode for Obs.4 (h) 2nd mode for Obs.4 (i) 3rd mode for Obs.4

Fig. 9 – The representative mode shapes calculated through eigen value analysis

5. Concluding remarks

Based on ambient vibration measurements for different construction stages, the detail modal properties of a two-story wooden house are identified through FDD technique, and the change in modal parameters are revealed. The identified mode shapes seemed to be relatively robust, however, the eigenfrequencies were not so clear in some cases. In addition, we constructed three-dimensional frame models based on limited information. The numerical model explained the observation-based modal properties, after adjusting the parameters with respect to mass. Mass estimation with high accuracy is necessary to discuss the detailed structural rigidity.

6. Acknowledgements

A part of this work was supported by JSPS KAKENHI Grant Numbers JP18K13817 and JP19H02400.

7. References

[1] Yasuda Y (1985): The variation of vibrational characteristics of a traditional wooden house under construction, *Summaries of technical papers of annual meeting Architectural Institute of Japan*, 21217, 1233-1234.

[2] Onozuka K, Ohashi Y. and Sakamoto I (1998) : Study of dynamic characteristics of wood-framed house subjected to microtremor, *Summaries of technical papers of annual meeting Architectural Institute of Japan*, **1998**, 219-220.

[3] Onozuka K, Harada N, Ohashi Y. and Sakamoto I (1999) : Study of dynamic characteristics of wood-framed house subjected to microtremor Part 2, *Summaries of technical papers of annual meeting Architectural Institute of Japan*, **1999**, 129-130.

[4] Harada N, Sakamoto I, Terui K, and Onozuka K (1999) : Study of dynamic characteristics of wood-framed house subjected to microtremor Part 3, *Summaries of technical papers of annual meeting Architectural Institute of Japan*, **1999**, 131-132.

[5] Tabata C and Ohashi Y (2007) : Microtremor measurement and possibility of its application to seismic diagnosis - Study on seismic diagnosis for wooden structures Part 2-, *J. Struct. Constr. Eng., AIJ,* 616, 141-147.

[6] Iwai S. (2007) : The relationship between earthquake-bearing wall area index, micro-tremor property and earthquake damage of conventional wooden-framed houses, Bulletin of Hiroshima University, **41**,61-65.

[7] Fukumoto Y and Koshihara M (2008) : Stiffness evaluation of existing wooden houses using microtremor observation, *Monthly journal of the Institute of Industrial Science, University of Tokyo*, **60**(2), 119-123.

[8] Sugino M, Ohmura S, Tokuoka S, and Hayashi Y (2016) : Maximum response evaluation of traditional wooden houses based on microtremor measurements, *J. Struct. Constr. Eng., AIJ,* **81**(729), 1869-1879.

[9] Brinker R, Zhang L, Anderson P (2001) : Modal Identification of Output-only Systems Using Frequency Domain Decomposition, *Smart Materials and Structures*, **10**, 441-445.

[10] Randall J A (2003) : The Modal Assurance Criterion – Twenty Years of Use and Abuse, *Sound and Vibration*, 14-20.

[11] Shimizu H, Mori T, Murase S, Tachibana K, Isoda H, Komatsu K, Yoshikawa S, and Fukuda Y (2009) : Weight appraisal of newly built wood house, *AIJ J. Technol. Des.*,**15** (29), 115-120.

[12] Ikeda Y (2008) : Mass identification for buildings on linear programming utilizing modal shapes, *J. Struct. Constr. Eng.*, *AIJ*, **73** (627), 749-756.

[13] Saito T (1998) : System identification of a high-rise building applying multi-input-multi-output ARX model of modal analysis, *J. Struct. Constr. Eng.*, *AIJ*, 508, 47-54.

